

Enhanced visible light photocatalytic activity of Cr³⁺-doped anatase TiO₂ nanoparticles synthesized by sol–gel method

H. M. Yadav¹ · T. V. Kolekar² · A. S. Barge³ · N. D. Thorat⁴ · S. D. Delekar⁵ ·
B. M. Kim¹ · B. J. Kim¹ · J. S. Kim¹

Received: 30 June 2015 / Accepted: 25 September 2015 / Published online: 1 October 2015
© Springer Science+Business Media New York 2015

Abstract The photocatalytic degradation of methylene blue (MB) has been investigated under visible light irradiation with an incandescent light bulb using chromium doped TiO₂ nanoparticles. Cr–TiO₂ photocatalysts were successfully synthesized by sol–gel method at room temperature and characterized by X-ray diffraction (XRD), UV–Vis diffuse reflectance spectroscopy (UV–Vis DRS), Raman spectroscopy, Transmission electron microscopy (TEM) and X-ray photoelectron spectroscopy. The band gap energy of the nanoparticles were estimated using UV–Vis DRS technique. With increasing Cr³⁺ cations content into TiO₂ host lattice, the optical absorption band tuned in the visible region. XRD and TEM results reveal uniform and crystalline anatase TiO₂ nanoparticles. The photodegradation of MB indicated that the photocatalytic activity of pure TiO₂ nanoparticles increased with increasing Cr³⁺ cations concentration.

1 Introduction

Semiconductor photocatalysis is a promising technology for solar water splitting and purification of air and water [1]. Among various candidates, TiO₂ is a versatile material and has attracted great attention as an excellent photocatalyst for photocatalytic disinfection and degradation of various environmental contaminants. It is considered to be an ideal photocatalyst as it is chemically inert, photostable, highly reactive and inexpensive [2, 3]. However, TiO₂ can only absorb ultraviolet (UV) light ($\lambda < 390$ nm) due to its wide band-gap (3.0–3.2 eV), leading to absorption in only a small region of the solar spectrum. The undesired recombination of photoexcited charge carriers limited the effective application of TiO₂. To avoid recombination by increasing the lifetime of e/h⁺ pairs and to lower the band gap, doping with metals, non-metals or a combination of both is usually performed [4–6].

Metal doping in TiO₂ for photocatalytic application has gained lot of attention since enhancing the visible light response by lowering the charge carrier recombination. It is well known that metal ions doping in TiO₂ can influence the intrinsic properties of the semiconductor photocatalyst by extending its photoresponse into the visible. Importantly, metal-doped TiO₂ facilitates electron-hole separation and promotes the interfacial electron transfer processes. The optical absorption edge of the different transition metal ion doped TiO₂ is found to shift from UV to visible region of electromagnetic spectrum of light. This red shift in metal-doped TiO₂ was attributed to the charge-transfer transition between the d electrons of the dopant and the conduction band (CB) of TiO₂ [7].

The report came in 2010, Choi et al. [8] studied the effect of 13 different single metal ion dopants Ag⁺, Rb⁺,

✉ J. S. Kim
jskim@uos.ac.kr

H. M. Yadav
hemrajy@gmail.com

¹ Department of Materials Science and Engineering, University of Seoul, Seoul 130-743, South Korea

² Rajarambapu Institute of Technology, Islampur, Sangli, M.S. 415 414, India

³ Department of Chemical Engineering, Institute of Chemical Technology, Nathalal Parekh Road, Matunga, Mumbai, M.S. 400019, India

⁴ Department of Molecular Cell Biology, Samsung Biomedical Research Institute, Sungkyunkwan University, Seoul 440-746, South Korea

⁵ Department of Chemistry, Shivaji University, Kolhapur, M.S. 416004, India

Ni²⁺, Co²⁺, Cu²⁺, V³⁺, Ru³⁺, Fe³⁺, Os³⁺, Y³⁺, La³⁺, Pt⁴⁺, Pt²⁺, Cr³⁺, and Cr⁶⁺ on visible light reactivity of TiO₂. Among the various transition metal ions, Cr has been mostly used as a dopant since Cr doping extends the photoresponse to visible-light range by narrowing the band gap [9–13]. Doping TiO₂ with Cr has found to promote photoelectrochemical water decomposition and photodegradation of organic compounds using solar energy [11]. Zhang et al. [14] investigated the photocatalytic activities of Cr/TiO₂ nanotubes prepared by the combination of sol-gel process with hydrothermal treatment. Buddee et al. [15] reported the improvement in the photocatalytic property of amorphous TiO₂ by doping it with Cr(III) and Fe(III) ions for methylene blue degradation. Choudhury et al. [16] investigated the effect of Cr-doping on the structural, optical and magnetic properties of TiO₂ nanoparticles. The photocatalytic behavior of chromium-doped titania and chromium supported on the surface of titania were studied by Ould-Chikh et al. [17].

However, despite the absorption in the visible-light region, chromium-doped TiO₂ has been found to be photocatalytically inactive. This has been explained by the creation of additional oxygen vacancies upon chromium doping, as vacancies might constitute recombination sites for electron-hole pairs [18]. Though, it has been reported that the Cr-doped TiO₂ show lower visible-light photocatalytic activity than other transition metal ions doped TiO₂ but the Cr-doped TiO₂ may even show lower UV-light photocatalytic activity than TiO₂ [15]. Various factors, such as the physicochemical properties of TiO₂ (including particle size and crystalline phase), preparation methods for doping and the organic probe for photocatalytic activity test, have been confirmed to influence the final results for photoactivity test [19].

To understand the aforementioned controversy, therefore, in this work Cr-doped TiO₂ nanoparticles have been prepared with various doping concentration by modified sol-gel method at room temperature. The structural, optical and photocatalytic properties of the doped nanoparticles were also investigated.

2 Materials and methods

2.1 Materials

Titanium(IV) isopropoxide and sodium dodecyl sulfate were purchased from Sigma Aldrich. Chromium(III) nitrate nonahydrate were from SD Fine Chemicals (Mumbai, India). Ammonia, ethanol and methylene blue from Dusan Pure Chemicals Co. Ltd Korea. Solutions were prepared using water from a Millipore Water Milli Q purification system. All chemicals used as received.

2.2 Synthesis of photocatalyst

The Cr-doped TiO₂ nanoparticles were synthesized with the slightly modified sol-gel method, which was reported previously [20]. In the preparation, titanium(IV) isopropoxide was mixed with glacial acetic acid and magnetically stirred for 5 min, and then aqueous solution of sodium dodecyl sulfate followed by 50 mL of deionized water was added and again stirred for 40 min. To get the desired concentration of Cr³⁺ ion as a dopant (1.0–3.0 mol%) in TiO₂, required stoichiometric amount of aqueous solution of Cr(NO₃)₃·9H₂O was then added and stirred for 60 min. Then 20 mL of ammonia solution was added and the mixture was further stirred at 60 °C for 2 h. The resulting product was filtered, washed with ethanol and dried at 110 °C in an oven. The catalyst was calcinated in air at 400 °C for 4 h. The different samples such as 1.0 mol% Cr-doped TiO₂, 2.0 mol% Cr-doped TiO₂, and 3.0 mol% Cr-doped TiO₂ are denoted as Cr1–TiO₂, Cr2–TiO₂ and Cr3–TiO₂, respectively.

2.3 Photocatalytic activity test

The photocatalytic activity of the prepared samples was evaluated with the degradation of MB under UV and visible light irradiations. In a glass beaker, 10 mg L⁻¹ of photocatalyst and 100 mL of MB (1.6 × 10⁻⁵ mol L⁻¹) were stirred magnetically. The distance between the applied lamps and the surface of MB solution was 15 cm. The photodegradation was carried out at 25 °C by using a 200 W incandescent lamp (NB 220-C 200 W, Lanxi China). A UV-cut-off filter was inserted just below the white light lamp to filter the UV radiations with wavelength λ < 410 nm. Prior to light irradiation the catalyst and MB solution were stirred magnetically in the dark for 45 min to reach adsorption equilibrium. At regular time intervals, 1.5 mL of the solution was aspirated and centrifuged. Concentration of residual solution was estimated using UV-Visible-NIR spectrophotometer (Shimadzu UV 3150). Since the degradation mechanism of MB is well known with high reliability, we have monitored photodegradation by using a UV-Vis spectrophotometer.

The photodegradation rate of MB was calculated by the following equation:

$$\% \text{ Degradation rate of MB} = (C_0 - C_t / C_0) \times 100 \quad (1)$$

where C₀ is the initial concentration of MB and C_t is the concentration of MB at the irradiation time t.

2.4 Characterizations

The prepared samples have been characterized by various techniques such as XRD, TEM, XPS, Energy Dispersive

X-ray Spectroscopy (EDS), Raman spectroscopy and UV–Vis diffuse reflectance spectroscopy. The powder X-ray diffraction patterns of the nanoparticles were recorded at room temperature on a Bruker D8-advance diffractometer using $\text{Cu K}\alpha$ ($\lambda = 1.5418 \text{ \AA}$) radiation to identify the crystal phase. The diffraction data were collected in the 2θ range of 10° – 90° in step scan mode at a rate of $3^\circ/\text{min}$. TEM images of the samples were obtained with a Tecnai F30 field emission transmission electron microscope operating at 300 kV. EDS analysis was carried out to estimate the elemental composition of the sample. UV–Vis diffuse reflectance absorbance spectra of the samples were recorded with a UV–visible spectrophotometer (UV3600, Shimadzu, Japan) in the range of 200–800 nm. Raman spectra of the samples were obtained with a Raman spectrometer of Bruker make at a Laser power of 16 mW with 256 scans. X-ray photoelectron spectroscopy (XPS) measurements were carried out to examine the valence states of chromium element in Cr–TiO₂ nanoparticles. The XPS spectra were recorded on a Physical Electronics 5600 Multi-technique System with monochromatic Al $\text{K}\alpha$ radiation.

3 Results and discussion

3.1 X-ray diffraction analysis

XRD patterns of TiO₂ and Cr-doped TiO₂ nanoparticles are shown in the Fig. 1. XRD was used to investigate phase structures and crystallite size of the prepared nanoparticles. The diffraction pattern of the all Cr-doped TiO₂ nanoparticles matches with the standard anatase TiO₂ (JCPDS 21-1272). All Cr-doped TiO₂ nanoparticles consist of

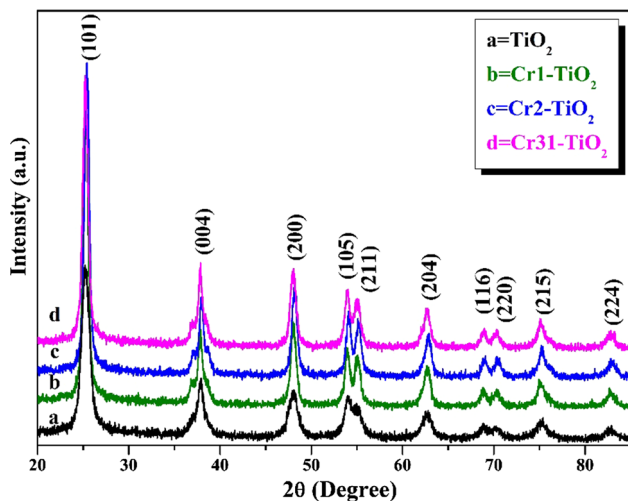


Fig. 1 XRD pattern of TiO₂ and Cr–TiO₂ nanoparticles

anatase as a unique phase. The crystallite size calculated by using Scherer's equation range from 12 to 14 nm. The diffraction pattern does not show any peak of secondary phase or other impurities such as chromium oxides. The peak position and intensity were not significantly affected by doping of Cr into the TiO₂ host lattice. The ionic radii of Cr³⁺ is 0.755 Å, which is very close to that of Ti⁴⁺ (0.745 Å), a TiO₂ crystalline lattice [8]. This shows that substitutional doping of Cr³⁺ occurred rather than interstitial doping in the Ti⁴⁺ sites.

3.2 UV–Vis diffuse reflectance spectroscopy

UV–Vis diffuse reflectance spectra of TiO₂ and Cr-doped TiO₂ nanoparticles are presented in Fig. 2. The sol–gel synthesized Cr-doped TiO₂ nanoparticles show absorption edge at 417, 436 and 477 nm for Cr1–TiO₂, Cr2–TiO₂ and Cr3–TiO₂ samples, respectively. The band gap energy values were determined by linear fitting the absorption edge. The band gap energy values were calculated to be 3.21, 3.0, 2.86 and 2.60 eV for TiO₂, Cr1–TiO₂, Cr2–TiO₂ and Cr3–TiO₂ samples, respectively. The increase of Cr ions contents in TiO₂ host lattice leads to linear increase in the optical absorption to the visible light region. The extended absorption in the visible region is due to the excitation of the electrons from the Cr to the conduction band of TiO₂. [8] The observed red shift in Cr–TiO₂ samples is consistent with the incorporation of Cr³⁺ into the titania matrix. The absorption spectra of the Cr–TiO₂ samples show more absorption than TiO₂ in the visible region, which indicates the existence of surface states. The oxygen vacancies should have been created to maintain charge neutrality due to metal doping, inducing bathochromic shift in the band gap transitions [12, 21].

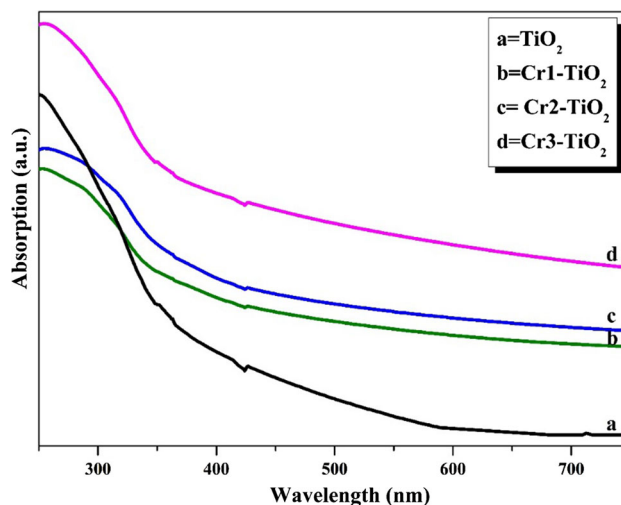


Fig. 2 UV–Vis diffuse reflectance spectra of TiO₂ and Cr–TiO₂ nanoparticles

Influence of doping on optical properties of TiO_2 is clearly evident in UV–Vis spectra and it is manifested by change of the color of doped samples from light to dark brown. The extended absorbance of Cr– TiO_2 nanoparticles into the visible region provides a possibility for enhancing the photocatalytic activity of TiO_2 for visible or solar light induced applications.

3.3 Raman spectroscopy

We carried out Raman spectroscopy experiments for further investigation of structural phases of TiO_2 and Cr-doped TiO_2 nanoparticles. Raman spectra of the samples are consistent with XRD data and suggests a pure phase as seen in Fig. 3. All samples exhibited a Raman peak pattern similar to the characteristic feature of anatase structured TiO_2 .

The tetragonal anatase structured titania belongs to D_{4h}^{19} ($I4_1/amd$) space group and may have following normal lattice vibration modes.

$$\text{Anatase} = A_{1g} + B_{1g} + B_{2g} + E_g \quad (2)$$

The strongest E_g mode at 145 cm^{-1} , arises due to the external vibration of the anatase structure is well resolved, which demonstrates that an anatase phase for all samples. A very small peak at 197 cm^{-1} is attributed to intrinsically weak vibrations in anatase TiO_2 . For all samples, the peaks at 147, 445 and 639 cm^{-1} belong to B_{1g} , E_g and A_{1g} modes, respectively. The peaks at 516 and 396 cm^{-1} can be attributed to B_{1g} and the peaks at 196, 144 cm^{-1} correspond to E_g vibration modes [22]. Interestingly, any peaks related to other oxides are not detected for Cr– TiO_2 nanoparticles. This reveals that the dopant is

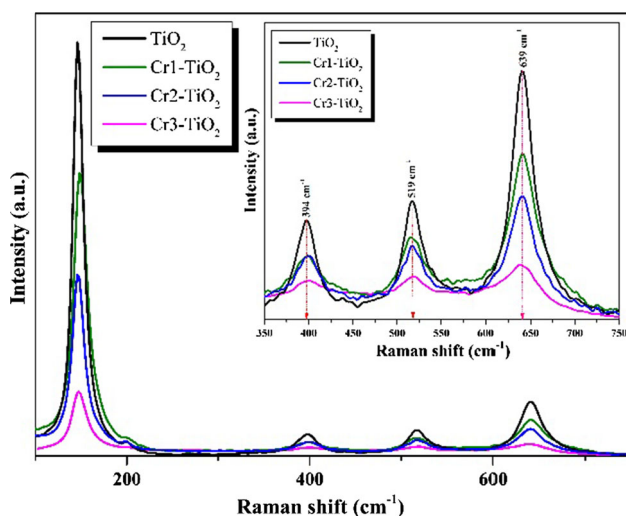


Fig. 3 Raman spectra of TiO_2 and Cr– TiO_2 nanoparticles

substitutionally interposed in the TiO_2 framework replacing Ti^{4+} cations. The absence of Raman bands (235 , 447 , and 612 cm^{-1}) corresponding to the rutile phase of TiO_2 again confirms the phase purity of the samples [23].

3.4 Transmission electron microscopy

A typical TEM image of TiO_2 and Cr3– TiO_2 nanoparticles can be seen in the Fig. 4. The diameters obtained from TEM analysis are in good agreement with those obtained from XRD analysis, which distribution from 7 to 14 nm. This demonstrates that the all Cr-doped TiO_2 nanoparticles were anatase crystalline, well dispersed and non-spherical shape. The selected area electron diffraction patterns (SAED) of TiO_2 and Cr3– TiO_2 are shown in inset of Fig. 4a, b, respectively. The bright spot in the center indicates that the electrons are diffracted randomly by the material and confirms crystalline nature of the TiO_2 and Cr3– TiO_2 nanoparticles [24].

The content of doped ions in the TiO_2 matrices was evaluated from EDS analysis. Figure 4c shows the elemental compositions of the representative Cr3– TiO_2 nanoparticles. From this figure, the peaks of corresponding dopant, Ti and O can be clearly seen, indicating that the nanoparticles contain dopants. Ti and O elements are found to be essentially pure and with the absence of any other impurities. All dopants of Cr were successfully identified, indicating that the doped metal ions have been integrated into TiO_2 host lattice. The obtained amount in EDS analysis was in good agreement with the doping contents.

3.5 X-ray photoelectron spectroscopy

XPS technique was used to study the surface chemistry of the Cr3– TiO_2 sample (Fig. 5a–d). In survey spectrum, peak observed at 284.6 eV corresponds to carbon impurities, arising due to the background of XPS test or the residual precursors [25].

The survey spectra for Cr3– TiO_2 sample exhibit presence of Ti, O, and Cr elements. The core level binding energies of Ti $2p_{3/2}$ and Ti $2p_{1/2}$ are observed at 463.56 eV and 457.87 eV , respectively which are in good agreement with standard binding energies of anatase TiO_2 [26]. The separation between the Ti $2p_{3/2}$ and Ti $2p_{1/2}$ peaks is 5.69 eV . These values are consistent with the values of Ti^{4+} cations of anatase TiO_2 [26]. The Cr $2p$ XPS spectrum showed a major peak at 576.93 eV and a minor peak at 585.71 eV . The peak can be assigned to Cr^{3+} [25]. Figure 5c show the XPS spectrum of O $1s$ configuration. The binding energies at 531.73 and 526.46 eV reveal the existence of surface hydroxyl groups of TiO_2 as well as O $1s$ of titanium lattice, respectively [27].

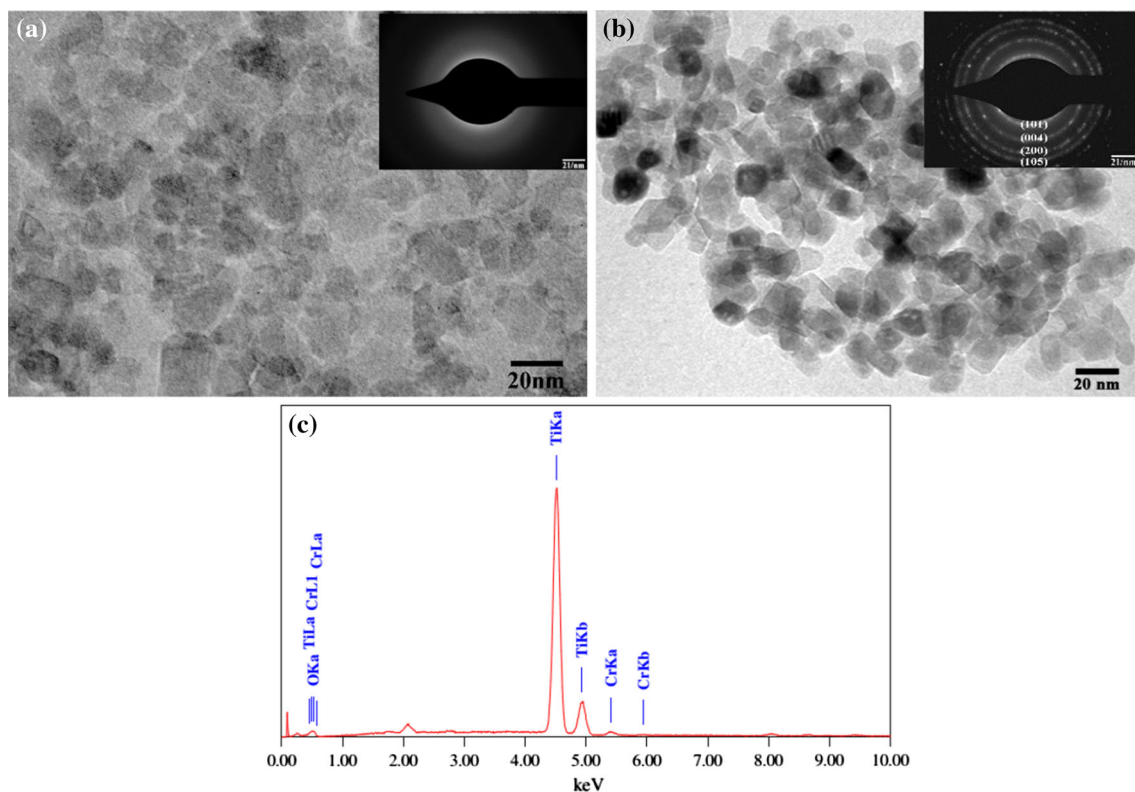


Fig. 4 TEM image of **a** TiO₂ and **b** Cr³⁺-TiO₂ nanoparticles (inset shows corresponding SAED pattern); **c** EDS of Cr³⁺-TiO₂ nanoparticles

3.6 Photodegradation of MB under visible light

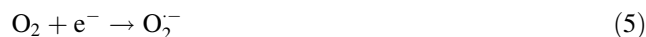
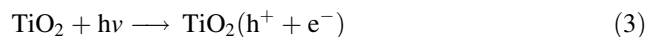
MB is a distinguished histological dye that has extensive applications in dyeing cottons, wools, temporary hair colorant, coloring papers and coating for paper stock [28, 29]. Although MB is not strongly dangerous, it can cause some harmful effects such as heart rate, shock, Heinz body formation, cyanosis, jaundice, vomiting, quadriplegia, and tissue necrosis in humans [30].

In this study, MB used as a model dye to demonstrate and compare the photocatalytic activity of metal modified TiO₂ nanoparticles. The photocatalytic degradation activity was tested with nanoparticles and a definite dye concentration (1.6×10^{-5} mol L⁻¹) under dark conditions and with visible light irradiations.

Figure 6 indicates the absorption spectra of Cr³⁺-TiO₂ nanoparticles which demonstrates the photodegradation of about 100 % of the MB solution after 10 h of the irradiation under visible light. It can be seen that about 20 % of the MB solution is mineralized under dark condition before irradiation of visible light.

The absorption maximum wavelength shift from 664 to 630 nm during the irradiation was observed. Such blue-shifted absorption is characteristic of N-demethylated derivatives of MB; the hypsochromic shifts occurred slowly. A mixture of N-demethylated analogs of MB

broadens the absorption spectra in the visible region [31]. Moreover, a parallel decrease in intensities and slight blue shift of the bands located at 292 nm was observed; these are caused by the N-demethylated degradation concomitantly with the degradation of the phenothiazine [32, 33]. The absorption of MB decreased with irradiation time due to photocatalytic degradation process under visible light. The plausible reaction mechanism for the photocatalytic degradation is given below.



The absorption of a photon with energy greater than the band gap of the TiO₂ excites a valence band electron to the conduction band, generating a positive hole in the valence band. The generated holes (h⁺) are trapped by H₂O and OH⁻ groups adsorbed on the surface of TiO₂ to generate hydroxyl radicals, and the electrons (e⁻) are attracted to the metal particle due to the difference in the work functions between TiO₂ and metal nanoparticles, thus preventing the recombination of photogenerated charge carriers [34, 35]. Hydroxyl radicals and superoxide anions produced by the photocatalytic process oxidize most of the organic compounds until complete decomposition is achieved [36, 37].

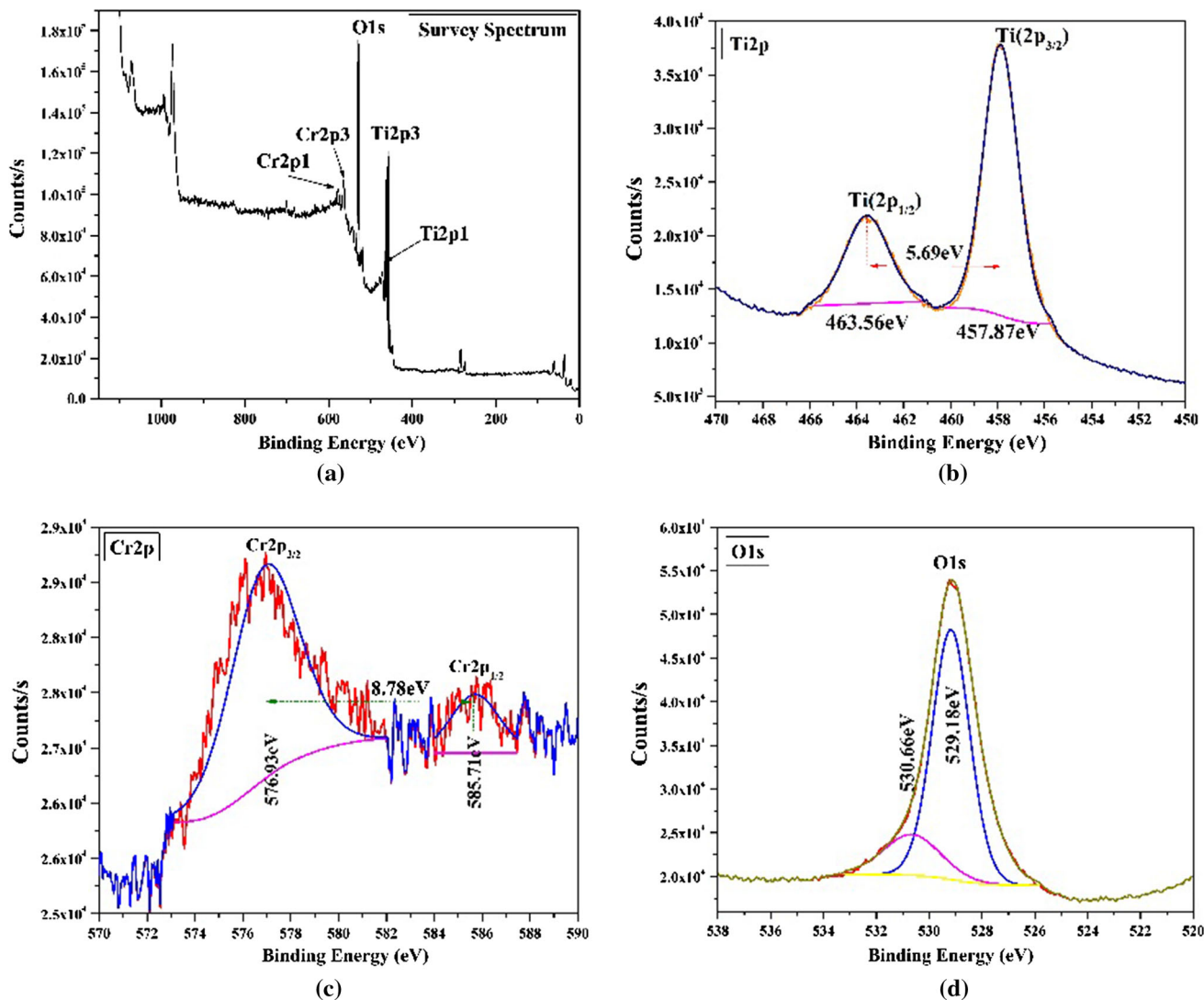


Fig. 5 XPS of Cr3–TiO₂ a survey spectrum, b Ti 2p, c Cr 2p, d O 1s

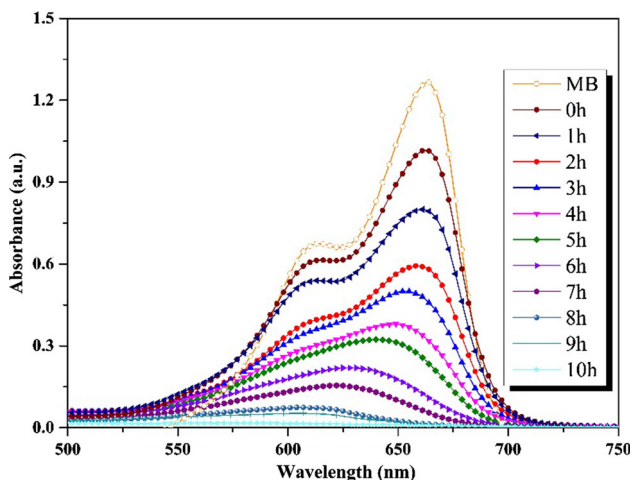
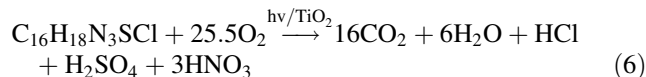


Fig. 6 Photodegradation of MB using Cr3–TiO₂ under visible light irradiation

Houas et al. [38] proposed that the decomposition of MB leads to the transformation of organic carbon into CO₂ while that of nitrogen and sulfur into inorganic ions. The resulting degradation process is as shown the equation below.



The photocatalytic activities of different samples are evaluated with the degradation rate of MB. Figure 7 shows the variation of the photocatalytic degradation using various samples estimated at the maximum absorption wavelength of MB (664 nm) with the time of irradiation. After 15 h exposure, blue color of MB solution completely vanished in the presence of Cr-doped TiO₂ nanoparticles under visible light irradiations. From figure it is observed that the

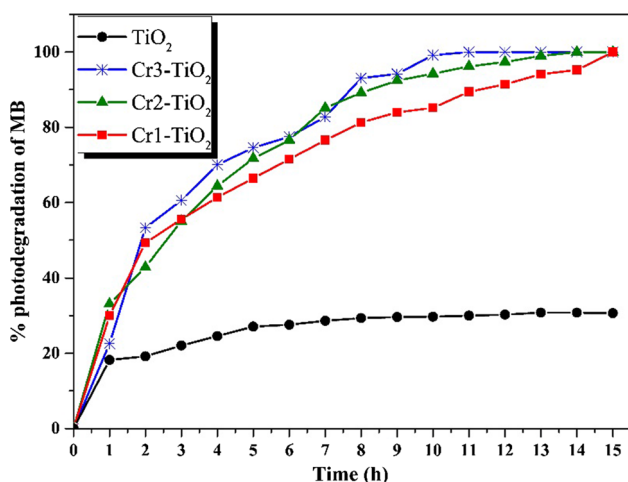


Fig. 7 Time dependent photodegradation of MB in presence of TiO_2 and Cr- TiO_2 nanoparticles under visible light irradiation

Cr3- TiO_2 exhibit much higher photocatalytic degradation of MB than other samples. This reveals that the photocatalytic activity of TiO_2 can be enhanced by the doping with chromium metal ions in the host lattice of TiO_2 .

As shown in Fig. 8, the degradation efficiency was impressed with increasing Cr doping. For Cr- TiO_2 , MB degradation rate depends on the Cr loading. Cr3- TiO_2 nanoparticles presented the highest activity with 100 % MB degradation at 10 h. In an extended time region, Cr1- TiO_2 and Cr2- TiO_2 were able to achieve complete MB degradation in about 13 and 15 h, respectively. Here, Cr3- TiO_2 nanoparticles had higher visible light photocatalytic activity and this can be correlated with the enhanced visible light absorption of TiO_2 by doping with 3.0 mol% chromium ions. The efficient absorption of visible light does not seem to be a key factor which controls the visible-

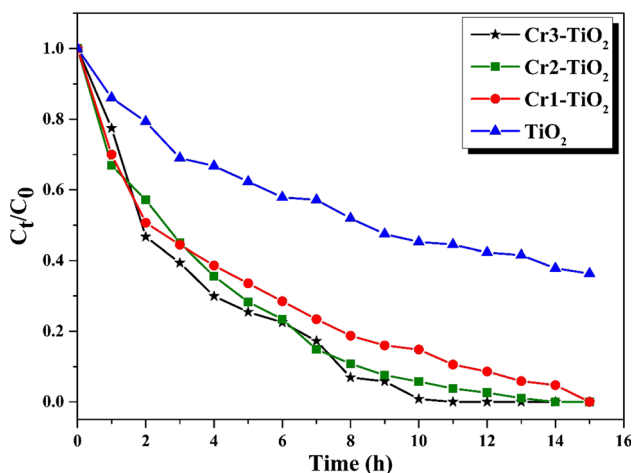


Fig. 8 Photocatalytic degradation of MB in presence of TiO_2 and Cr- TiO_2 nanoparticles

light photocatalytic activity of metal ion doped TiO_2 . Although to initiate photoreactions a visible-light absorption is obviously essential [8]. The variable activity of Cr-doped TiO_2 nanoparticles may be due to the dopant concentration. The concentration of dopant should be considered here, since a high concentration of Cr^{3+} in TiO_2 may induce over-trapping of holes with Cr^{3+} , which retards the recombination of photogenerated charge carriers [9]. The photocatalytic activity of metal ion doped TiO_2 strongly depends on the crystalline nature, phase composition, morphology, chemical composition, band gap, energy, surface area, particle size, electron-hole recombination rate, the existence of several dopants ions and synthesis methodology [39–42].

The photoactivity can be enhanced by doping TiO_2 with metal ions for improving the trapping-to-recombination rate ratio. However, when metal ions are incorporated into TiO_2 host lattice, the impurity energy levels formed in the band gap of TiO_2 can also lead to decrease the rate of recombination between photogenerated charge carriers. Not all metal doped TiO_2 photocatalyst will exhibit positive effects. The dopant content directly influences the rate of electron and hole recombination [43]. There is an optimum concentration of dopant ions where the thickness of the space-charge layer is similar to the depth of light penetration.

The dopants like Cr^{3+} and Fe^{3+} ions at a low concentration promote the separation of photogenerated charge carriers, which benefit the photocatalytic reaction. Conversely, the reaction between metal ions and electrons are rapidly enhanced at higher concentration of dopants, which is disadvantageous to photocatalytic reaction [15]. The present investigation reveals that the addition of optimum concentration of chromium ion into TiO_2 host lattice can tune the photocatalytic activity in the visible region of electromagnetic spectrum.

4 Conclusions

Cr doped anatase TiO_2 nanoparticles with visible light activity were successfully synthesized by modified sol-gel method at room temperature. XRD and Raman analysis of Cr- TiO_2 nanoparticles show characteristic features of nanocrystalline TiO_2 in tetragonal anatase phase. The effect of low concentration chromium doping on the photocatalytic activity of TiO_2 was investigated by performing the photodegradation of MB. The presence of chromium dopant plays a vital role in altering physiochemical and photocatalytic properties of TiO_2 . The optical band gap energy of Cr-doped TiO_2 nanoparticles shifted in the visible light region. XPS analysis confirmed the proper substitution of Ti^{4+} cations by Cr^{3+} cations in the TiO_2 matrix.

Cr–TiO₂ nanoparticles showed higher photoactivity than undoped samples. The photocatalytic degradation of MB is enhanced with increasing chromium concentration in TiO₂ host lattice. The doping of Cr³⁺ cations into TiO₂ facilitated its photocatalytic activity under visible light irradiation. Considering facile preparation process and visible light activity at low dopant concentration, Cr-doped TiO₂ photocatalyst are found to be plausibly applicable for environmental remediation applications.

Acknowledgments This research work was supported by a grant (14CTAP-C077607-01) from Infrastructure and transportation technology promotion research program funded by Ministry of Land, Infrastructure and Transport of Korean government.

References

- D.P. Macwan, P.N. Dave, S. Chaturvedi, A review on nano-TiO₂ sol–gel type syntheses and its applications. *J. Mater. Sci.* **46**, 3669–3686 (2011)
- D.F. Ollis, E. Pelizzetti, N. Serpone, Photocatalyzed destruction of water contaminants. *Environ. Sci. Technol.* **25**, 1522–1529 (1991)
- Y. Yalçın, M. Kılıç, Z. Çınar, Fe³⁺-doped TiO₂: a combined experimental and computational approach to the evaluation of visible light activity. *Appl. Catal. B Environ.* **99**, 469–477 (2010)
- J. Virkutyte, R.S. Varma, Visible light activity of Ag-loaded and guanidine nitrate-doped nano-TiO₂: degradation of dichlorophenol and antibacterial properties. *RSC Adv.* **2**, 1533–1539 (2012)
- S.S. Soni, G.S. Dave, M.J. Henderson, A. Gibaud, Visible light induced cell damage of Gram positive bacteria by N-doped TiO₂ mesoporous thin films. *Thin Solid Films* **531**, 559–565 (2013)
- S.S. Soni, M.J. Henderson, J.F. Bardeau, A. Gibaud, Visible-light photocatalysis in titania-based mesoporous thin films. *Adv. Mater.* **20**, 1493–1498 (2008)
- J.C.S. Wu, C.H. Chen, A visible-light response vanadium-doped titania nanocatalyst by sol–gel method. *J. Photochem. Photobiol. A Chem.* **163**, 509–515 (2004)
- J. Choi, H. Park, M.R. Hoffmann, Effects of single metal-ion doping on the visible-light photoreactivity of TiO₂. *J. Phys. Chem. C* **114**, 783–792 (2010)
- J. Zhu, Z. Deng, F. Chen, J. Zhang, H. Chen, M. Anpo et al., Hydrothermal doping method for preparation of Cr³⁺-TiO₂ photocatalysts with concentration gradient distribution of Cr³⁺. *Appl. Catal. B Environ.* **62**, 329–335 (2006)
- P. Bouras, E. Stathatos, P. Lianos, Pure versus metal-ion-doped nanocrystalline titania for photocatalysis. *Appl. Catal. B Environ.* **73**, 51–59 (2007)
- C.C. Tsai, H. Teng, Chromium-doped titanium dioxide thin-film photoanodes in visible-light-induced water cleavage. *Appl. Surf. Sci.* **254**, 4912–4918 (2008)
- A.T. Vu, Q.T. Nguyen, T.H.L. Bui, M.C. Tran, T.P. Dang, T.K.H. Tran, Synthesis and characterization of TiO₂ photocatalyst doped by transition metal ions (Fe³⁺, Cr³⁺ and V⁵⁺). *Adv. Nat. Sci. Nanosci. Nanotechnol.* **1**, 015009 (2010)
- X. Li, Z. Guo, T. He, The doping mechanism of Cr into TiO₂ and its influence on the photocatalytic performance. *Phys. Chem. Chem. Phys.* **15**, 20037–20045 (2013)
- S. Zhang, Y. Chen, Y. Yu, H. Wu, S. Wang, B. Zhu et al., Synthesis, characterization of Cr-doped TiO₂ nanotubes with high photocatalytic activity. *J. Nanoparticle Res.* **10**, 871–875 (2007)
- S. Buddee, S. Wongnawa, U. Sirimahachai, W. Puetpaibool, Recyclable UV and visible light photocatalytically active amorphous TiO₂ doped with M(III) ions (M = Cr and Fe). *Mater. Chem. Phys.* **126**, 167–177 (2011)
- B. Choudhury, A. Choudhury, Structural, optical and ferromagnetic properties of Cr doped TiO₂ nanoparticles. *Mater. Sci. Eng., B* **178**, 794–800 (2013)
- S. Ould-Chikh, O. Proux, P. Afanasiev, L. Khrouz, M.N. Hedhili, D.H. Anjum et al., Photocatalysis with chromium-doped TiO₂: bulk and surface doping. *ChemSusChem* **7**, 1361–1371 (2014)
- R. Bechstein, M. Kitta, J. Schütte, H. Onishi, A. Kühnle, The effects of antimony doping on the surface structure of rutile TiO₂(110). *Nanotechnology* **20**, 264003 (2009)
- Z. Zhang, C. Wang, R. Zakaria, J.Y. Ying, Role of particle size in nanocrystalline TiO₂-based photocatalysts. *J. Phys. Chem.* **102**, 10871–10878 (1998)
- S.D. Delekar, H.M. Yadav, S.N. Achary, S.S. Meena, S.H. Pawar, Structural refinement and photocatalytic activity of Fe-doped anatase TiO₂ nanoparticles. *Appl. Surf. Sci.* **263**, 536–545 (2012)
- H.M. Yadav, S.V. Otari, R.A. Bohara, S.S. Mali, S.H. Pawar, S.D. Delekar, Synthesis and visible light photocatalytic antibacterial activity of nickel-doped TiO₂ nanoparticles against Gram-positive and Gram-negative bacteria. *J. Photochem. Photobiol. A Chem.* **294**, 130–136 (2014)
- J.S. Chen, Y.L. Tan, C.M. Li, Y.L. Cheah, D. Luan, S. Madhavi et al., Constructing hierarchical spheres from large ultrathin anatase TiO₂ nanosheets with nearly 100 % exposed (001) facets for fast reversible lithium storage. *J. Am. Chem. Soc.* **132**, 6124–6130 (2010)
- K. Bhattacharyya, S. Varma, A.K. Tripathi, S.R. Bharadwaj, A.K. Tyagi, Effect of vanadia doping and its oxidation state on the photocatalytic activity of TiO₂ for gas-phase oxidation of ethene. *J. Phys. Chem. C* **112**, 19102–19112 (2008)
- Y. Yu, X. Yin, A. Kvit, X. Wang, Evolution of hollow TiO₂ nanostructures via the Kirkendall effect driven by cation exchange with enhanced photoelectrochemical performance. *Nano Lett.* **14**, 2528–2535 (2014)
- C.D. Wagner, W.M. Riggs, L.E. Davis, J.F. Moulder, G.E. Muilenberg, *Handbook of X-Ray Photoelectron Spectroscopy* (Perkin-Elmer Corp., Physical Electronics Division, USA, 1979)
- J. Zhu, F. Chen, J. Zhang, H. Chen, M. Anpo, Fe³⁺-TiO₂ photocatalysts prepared by combining sol–gel method with hydrothermal treatment and their characterization. *J. Photochem. Photobiol. A Chem.* **180**, 196–204 (2006)
- L. Li, C. Liu, Y. Liu, Study on activities of vanadium (IV/V) doped TiO₂(R) nanorods induced by UV and visible light. *Mater. Chem. Phys.* **113**, 551–557 (2009)
- J.P. Tardivo, A. Del Giglio, C.S. de Oliveira, D.S. Gabrielli, H.C. Junqueira, D.B. Tada et al., Methylene blue in photodynamic therapy: from basic mechanisms to clinical applications. *Photodiagn. Photodyn. Ther.* **2**, 175–191 (2005)
- B.H. Hameed, A.A. Ahmad, Batch adsorption of methylene blue from aqueous solution by garlic peel, an agricultural waste biomass. *J. Hazard. Mater.* **164**, 870–875 (2009)
- Y. Bulut, H. Aydın, A kinetics and thermodynamics study of methylene blue adsorption on wheat shells. *Desalination* **194**, 259–267 (2006)
- T. Zhang, T. Oyama, A. Aoshima, H. Hidaka, J. Zhao, N. Serpone, Photooxidative N-demethylation of methylene blue in aqueous TiO₂ dispersions under UV irradiation. *J. Photochem. Photobiol. A Chem.* **140**, 163–172 (2001)
- F. Wang, S. Min, Y. Han, L. Feng, Visible-light-induced photocatalytic degradation of methylene blue with polyaniline-sensitized composite photocatalysts. *Superlattices Microstruct.* **48**, 170–180 (2010)
- T. Mohammad, H. Morrison, Simultaneous photoconjugation of methylene blue and cis-Rh(phen)₂Cl₂⁺ to DNA via a synergistic effect†. *Photochem. Photobiol.* **71**, 369–381 (2007)

34. P. Sangpour, F. Hashemi, A.Z. Moshfegh, Photoenhanced degradation of methylene blue on cosputtered M:TiO₂ (M = Au, Ag, Cu) nanocomposite systems: a comparative study. *J. Phys. Chem. C* **114**, 13955–13961 (2010)
35. M.R. Hoffmann, S.T. Martin, W. Choi, D.W. Bahnemannt, Environmental applications of semiconductor photocatalysis. *Chem. Rev.* **95**, 69–96 (1995)
36. M.B. Fisher, D.A. Keane, P. Fernández-Ibáñez, J. Colreavy, S.J. Hinder, K.G. McGuigan et al., Nitrogen and copper doped solar light active TiO₂ photocatalysts for water decontamination. *Appl. Catal. B Environ.* **130–131**, 8–13 (2013)
37. M. Pelaez, N.T. Nolan, S.C. Pillai, M.K. Seery, P. Falaras, A.G. Kontos et al., A review on the visible light active titanium dioxide photocatalysts for environmental applications. *Appl. Catal. B Environ.* **125**, 331–349 (2012)
38. A. Houas, H. Lachheb, M. Ksibi, E. Elaloui, C. Guillard, J.M. Herrmann, Photocatalytic degradation pathway of methylene blue in water. *Appl. Catal. B Environ.* **31**, 145–157 (2001)
39. B. Ohtani, Y. Ogawa, S. Nishimoto, Photocatalytic activity of amorphous-anatase mixture of titanium(IV) oxide particles suspended in aqueous solutions. *J. Phys. Chem. B.* **5647**, 3746–3752 (1997)
40. U.G. Akpan, B.H. Hameed, Parameters affecting the photocatalytic degradation of dyes using TiO₂-based photocatalysts: a review. *J. Hazard. Mater.* **170**, 520–529 (2009)
41. S. Liu, J.-H. Yang, J.-H. Choy, Microporous SiO₂-TiO₂ nanosols pillared montmorillonite for photocatalytic decomposition of methyl orange. *J. Photochem. Photobiol. A Chem.* **179**, 75–80 (2006)
42. M.A. Rauf, S.B. Bukallah, A. Hamadi, A. Sulaiman, F. Hamadi, The effect of operational parameters on the photoinduced decoloration of dyes using a hybrid catalyst V₂O₅/TiO₂. *Chem. Eng. J.* **129**, 167–172 (2007)
43. J.M. Herrmann, Heterogeneous photocatalysis: fundamentals and applications to the removal of various types of aqueous pollutants. *Catal. Today* **53**, 115–129 (1999)